Available online at www.sciencedirect.com
ScienceDirect
Journal of the European Ceramic Society 30 (2010) 3445–3453
www.elsevier.com/locate/jeurceramsoc

Structural properties of $(Bi_{0.5}Na_{0.5})_{1-x}Ba_xTiO_3$ lead-free piezoelectric ceramics

Gunnar Picht [a], Jörg Töpfer [a,*], Eberhard Hennig [b]

[a] *University of Applied Sciences Jena, Dept. SciTec, Carl-Zeiss-Promenade 2, 07745 Jena, Germany*
[b] *PI Ceramic GmbH, Lindenstraße, 07589 Lederhose, Germany*

Received 19 March 2010; received in revised form 19 July 2010; accepted 28 July 2010
Available online 21 August 2010

Abstract

A systematic XRD investigation of poled and unpoled ceramics of the system $(1-x)\,Bi_{0.5}Na_{0.5}TiO_3$–$x\,BaTiO_3$ $(0 \le x \le 0.2)$ (BNBT) was performed. The variation of the lattice parameters confirms the existence of a morphotropic phase boundary at $0.06 \le x \le 0.08$; however, significant differences in unit cell parameters between poled and unpoled states appear. Lattice distortions of the rhombohedral and tetragonal phases are significantly increased in poled samples. Dramatic changes in peak intensities of the pseudo-cubic (2 0 0) reflections between poled and unpoled samples reveal a strong enhancement of the tetragonal volume fraction in the poled state. Temperature-dependent XRD studies confirm a transition into a cubic high-temperature phase. This transition is rather smooth in the unpoled state. In poled samples, the tetragonal distortion and the tetragonal volume fraction display a different temperature variation and tetragonal regions seem to persist into the cubic phase field.

Keywords: Lead-free piezoelectric ceramics; BNBT; Morphotropic phase boundary

1. Introduction

Piezoelectric materials based on the $Pb(Zr/Ti)O_3$ (PZT) system play an important role in displacement transducers (actuators), accelerators, piezoelectric motors, resonators and ultrasonic devices.[1] Due to environmental regulations, an enormous research effort devoted to the development of lead-free piezoelectric materials has been generated in the last decade. However, to date no material system with electromechanical properties comparable to PZT has been discovered yet.[2,3] One of the potential candidate materials for commercial lead-free piezoelectrics is the system $(1-x)\,Bi_{0.5}Na_{0.5}TiO_3$–$x\,BaTiO_3$ $(0 \le x \le 0.2)$ (BNBT), which exhibits a morphotropic phase boundary (MPB) at $0.06 \le x \le 0.08$ with good piezoelectric and electromechanical properties at the MPB.[4–6] Other, more complex piezoelectric systems based on (or similar to) BNBT have also been explored, e.g. $Bi_{0.5}K_{0.5}TiO_3$–$BaTiO_3$ (NKBT),[7] $Bi_{0.5}Na_{0.5}TiO_3$–$Bi_{0.5}K_{0.5}TiO_3$–$BaTiO_3$ (BNKBT),[8,9] $Bi_{0.5}Na_{0.5}TiO_3$–$BaTiO_3$–$SrTiO_3$ (BNBST)[10] and $Bi_{0.5}Na_{0.5}TiO_3$–$BaTiO_3$–$K_{0.5}Na_{0.5}NbO_3$ (BNBT–KNN).[11] Since all these advanced systems rely on the basic phenomena of the BNBT system, a thorough understanding of the structural, dielectric, piezoelectric and electromechanical properties including its temperature behaviors is required. The temperature-dependences of the dielectric and electromechanical properties are fairly well documented,[4,12,13] however, information about the temperature-dependent series of structural phase transitions and the corresponding phase diagram are scarce.[4] The structural properties of the end member $Bi_{0.5}Na_{0.5}TiO_3$ (BNT) have already been studied earlier: BNT exhibits two structural phase transitions from a ferroelectric rhombohedral to a tetragonal phase at about 250 °C and further to a paraelectric cubic phase at about 540 °C.[14,15] BNT exhibits a wide temperature window (260–420 °C) with coexisting rhombohedral and tetragonal phases.[16] For the BNBT system, systematic XRD investigations on phase transitions and the temperature dependence of the MPB are not available. Suchanicz et al.[17] have performed X-ray diffraction measurements of selected compositions as function

* Corresponding author. Tel.: +49 3641 205350; fax: +49 3641 205451.
E-mail address: joerg.toepfer@fh-jena.de (J. Töpfer).

0955-2219/$ – see front matter © 2010 Elsevier Ltd. All rights reserved.
doi:10.1016/j.jeurceramsoc.2010.07.042

of temperature; for $x = 0.12$ they report a tetragonal to cubic transition at 220 °C.

To further optimize BNBT ceramics, an understanding of the behavior under an applied electric field (e.g. during poling) is desirable. The influence of an electric field on the strain of a piezoelectric material is usually considered to consist of two contributions: (i) piezoelectric strain due to changes in the lattice spacing (intrinsic contribution), which can be monitored in XRD experiments by a shift of peak positions and (ii) non-180° domain switching (extrinsic contribution), which is detected by changes in peak intensities of specific diffraction peaks. This behavior has been studied in great detail for PZT ceramics.[18,19] For BNBT materials, detailed XRD investigations, neither in situ XRD measurements under applied electric fields, nor ex situ measurements on poled and unpoled samples, have not been reported yet. In the present XRD investigation of piezoelectric lead-free ceramics of the system $(1-x)$ $Bi_{0.5}Na_{0.5}TiO_3$–x $BaTiO_3$ ($0 \leq x \leq 0.2$) (BNBT) we have addressed the following topics: (i) variation of the room-temperature structural properties (lattice parameters, lattice distortions, phase volume fractions) for poled and unpoled samples and (ii) temperature-dependent phase transformation behavior of poled and unpoled samples.

2. Experimental

Twenty compositions of $(Bi_{0.5}Na_{0.5})_{1-x}Ba_xTiO_3$ with $0 \leq x \leq 0.20$ (sample notation: e.g. BNBT20 for $x = 0.20$) were prepared by the mixed oxide route. The starting materials $BaCO_3$, Na_2CO_3, Bi_2O_3 and TiO_2 were mixed in isopropanol, calcined at 800–950 °C for 2 h and fine milled in a planetary ball mill. Samples of 20 mm diameter and 2 mm height were uniaxially pressed. After binder burnout, the pellets were sintered at 1080–1200 °C for 2 h in air.

The sintered samples show a high density of more than 98% of the theoretical density. The microstructure of the samples was determined on polished and etched samples by secondary electron microscopy (SEM) with a Zeiss DSM 900. The grain size of the samples is about 2–4 μm. The sintered discs were ground to a diameter of 15 mm and a thickness of 0.5 mm. To remove any stress from the mechanical treatment the samples were heated to 850 °C and then poled in an oil bath at 80 °C by applying an electric field of 5 kV/mm for 15 min; poling was performed without electrodes by placing the samples between two metal plates (this sample set is referred to as poled samples). In order to remove the texture from poling the discs were heated for 5 h at 850 °C (referred to as unpoled samples). XRD investigations of the unpoled and poled states were performed on the same specimen.

The X-ray diffraction (XRD) measurements were performed with a Siemens D5000 diffractometer with Bragg–Brentano geometry, a graphite secondary monochromator and CuK_α radiation. The measurements were made at 45 kV and 30 mA with a step size of 0.01° and 9 s/step in the range of 20–70° 2θ. The lattice parameters were calculated with the software AFPAR based on a least square refinement routine. The lattice parameters of the rhombohedral perovskites were refined in a hexagonal setting and then transferred into parameters of a primitive rhombohedral cell ($Z = 2$) using the expressions[20,21]:

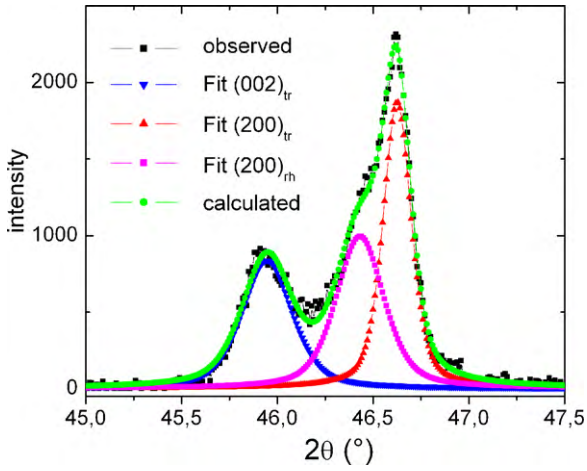

Fig. 1. Example of single-peak fitting of the pseudo-cubic (2 0 0) peak of a composition in the MPB region ($x = 0.08$).

$$a_{\mathrm{rhpr}} = \sqrt{\frac{a_{\mathrm{hex}}^2}{3} + \frac{c_{\mathrm{hex}}^2}{9}} \quad \text{and} \quad \sin\frac{\alpha_{\mathrm{rhpr}}}{2} = \frac{1}{2\sqrt{\frac{1}{3} + \frac{(c_{\mathrm{hex}}/a_{\mathrm{hex}})^2}{9}}} \tag{1}$$

These rhombohedral parameters were subsequently transformed into unit cell parameters of a face-centered rhombohedral cell ($Z = 8$) using:

$$a_{\mathrm{rhfc}} = a_{\mathrm{rhpr}}\sqrt{3 - 2\cos\alpha_{\mathrm{rhpr}}} \text{ and } \cos\alpha_{\mathrm{rhfc}} = \frac{2\cos\alpha_{\mathrm{rhpr}} - 1}{3 - 2\cos\alpha_{\mathrm{rhpr}}} \tag{2}$$

The pseudo-cubic unit cell length a_{rh} was obtained from $a_{\mathrm{rhfc}}/2$ and $\alpha_{\mathrm{rh}} = \alpha_{\mathrm{rhfc}}$. The lattice distortion of the tetragonal unit cell was calculated using $\delta_{\mathrm{tr}} = (c/a) - 1$. The distortion of the rhombohedral cell is $\delta_{\mathrm{rh}} = (9/8)[d_{1\,1\,1}/d_{-1\,1\,1}] - 1$.

To evaluate the tetragonal or rhombohedral phase contents, the tetragonal (0 0 2) and (2 0 0) reflections (44.5–47.5° 2θ) and the rhombohedral (pseudo-cubic) (1 1 1)/(−1 1 1) peaks (39.0–41.0° 2θ) were measured with a slow scan rate (25 s/step). The peak positions and intensities were analyzed with the software package Peakfit (SeaSolve Software Inc.) using a symmetric Gauss–Lorentz profile function. Fig. 1 shows as an example the pseudo-cubic (2 0 0) reflection of a composition at the morphotropic phase boundary; the observed pattern is well resolved into the tetragonal (0 0 2) and (2 0 0) and the rhombohedral (pseudo-cubic) (2 0 0) peaks. The tetragonal volume fraction was calculated using the formula:

$$V_{\mathrm{tr}}(\%) = \frac{I_{\mathrm{tr}(0\,0\,2)} + I_{\mathrm{tr}(2\,0\,0)}}{I_{\mathrm{rh}(2\,0\,0)} + I_{\mathrm{tr}(0\,0\,2)} + I_{\mathrm{tr}(2\,0\,0)}} \times 100 \tag{3}$$

The rhombohedral volume fraction is $V_{\mathrm{rh}} = 1 - V_{\mathrm{tr}}$.

High-temperature XRD measurements were performed in a MRI temperature chamber with the studied pellet mounted onto a PtRh heating strip. Samples were heated with 10 K/min up to a given temperature and held there for 20 min before the start

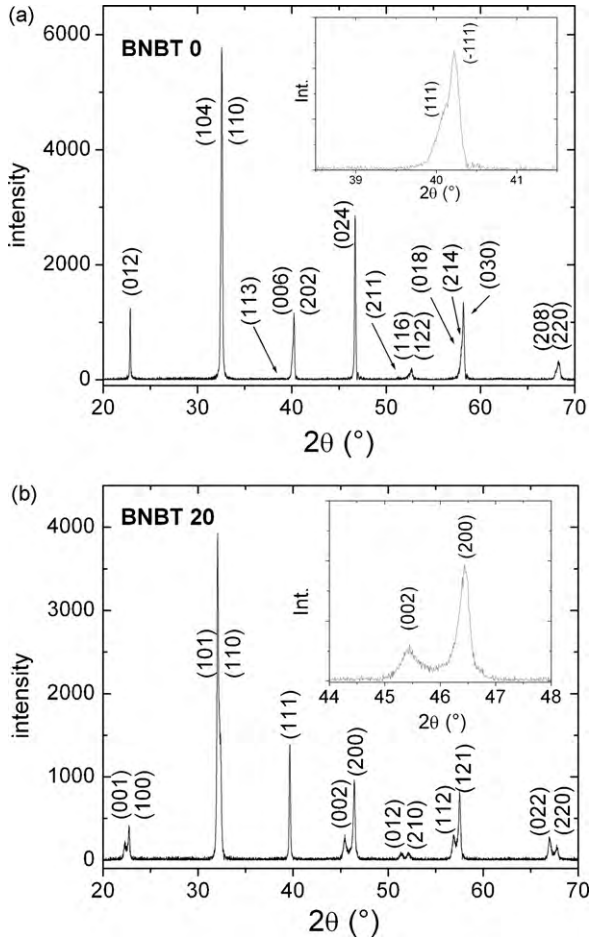

Fig. 2. XRD patterns of unpoled samples of a representative rhombohedral (BNBT 0; hexagonal unit cell setting) (a) and tetragonal composition (BNBT 20) (b); insets: pseudo-cubic (1 1 1) and (2 0 0) peaks.

of the XRD run. The temperature was measured with a Pt/Rh thermocouple directly connected to the heating strip below the pellets.

3. Results

3.1. Room-temperature XRD studies of poled and unpoled samples

All sintered ceramics exhibit a perovskite-type structure without any secondary or impurity phases. Fig. 2 shows the diffraction patterns of unpoled samples of BNBT 0 and BNBT 20 as representative examples of compositions with rhombohedral and tetragonal perovskite structures, respectively. $Bi_{0.5}Na_{0.5}TiO_3$ (BNT, BNBT0) has a rhombohedral structure (space group R3c) at room temperature.[14] The X-ray diffractogram of BNT (Fig. 2a) is typical of a rhombohedrally distorted perovskite. The insets show details of the peaks at around $2\theta = 40$ demonstrating a characteristic splitting of the cubic (1 1 1) reflection into pseudo-cubic (1 1 1) and (−1 1 1) or into rhombohedral (0 0 6) and (2 0 2) peaks. The unit cell parameters (Table 1) of the unpoled sample of $Bi_{0.5}Na_{0.5}TiO_3$ (BNT, BNBT0) very well agree with those of BNT from Ref. [14]. The other end member

Table 1
Room-temperature lattice parameters a, c (Å) and α (°) of the system $(1-x)$ $Bi_{0.5}Na_{0.5}TiO_3$–x $BaTiO_3$ with $0 \le x \le 0.2$ (0–20 mol% BT).

BT (mol%)	Unpoled						Poled					
	a_{hex}	c_{hex}	a_{rh}	α_{rh}	a_{tr}	c_{tr}	a_{hex}	c_{hex}	a_{rh}	α_{rh}	a_{tr}	c_{tr}
0	5.4863 (9)	13.5116 (21)	3.8867 (7)	89.84 (2)	–	–	5.4837 (6)	13.5630 (14)	3.8902 (1)	89.70 (1)	–	–
2	5.4893 (10)	13.5331 (22)	3.8899 (2)	89.80 (1)	–	–	5.4884 (9)	13.5718 (20)	3.8932 (3)	89.71 (1)	–	–
3	5.4920 (5)	13.5378 (11)	3.8916 (1)	89.81 (1)	–	–	5.4933 (5)	13.5919 (13)	3.8975 (2)	89.69 (1)	–	–
4	5.4957(7)	13.5492 (16)	3.8945 (2)	89.80 (1)	–	–	5.4967 (8)	13.5918 (18)	3.8991 (2)	89.72 (1)	3.9140 (19)	3.9298 (22)
5	5.4999 (9)	13.5514 (21)	3.8968 (3)	89.82 (1)	–	–	5.4998 (5)	13.5973 (11)	3.9011 (1)	89.72 (1)	3.9101 (19)	3.9465 (19)
6	5.4967 (8)	13.5918 (18)	3.8991 (2)	89.70 (1)	3.9036 (12)	3.9205 (13)	5.4997 (14)	13.6098 (33)	3.9022 (11)	89.74 (3)	3.8933 (8)	3.9480 (8)
7	5.5089 (11)	13.57632 (24)	3.9033 (4)	89.81 (2)	3.9004 (8)	3.9325 (8)	5.5017 (42)	13.6101 (53)	3.9033 (13)	89.70 (3)	3.8912 (7)	3.9467 (7)
8	5.5016 (17)	13.5752 (39)	3.9067 (12)	89.80 (4)	3.8949 (6)	3.9464 (7)			–	–	3.8905 (3)	3.9587 (3)
9	5.5122 (28)	13.5927 (63)	3.9076 (10)	89.80 (4)	3.8937 (3)	3.9521 (3)			–	–	3.8917 (3)	3.9620 (3)
10	5.5193 (38)	13.6290 (87)	3.9133 (9)	89.70 (6)	3.8947 (3)	3.9577 (3)			–	–	3.8921 (3)	3.9683 (3)
12			–	–	3.8982 (2)	3.9674 (3)			–	–	3.8956 (2)	3.9777 (2)
16			–	–	3.9046 (2)	3.9808 (2)			–	–	3.9023 (5)	3.9901 (6)
20			–	–	3.9078 (3)	3.9877 (3)			–	–	3.9090 (8)	4.0002 (9)

$BaTiO_3$ has a tetragonal room-temperature cell (space group P4mm). Tetragonal BNBT compositions studied in this work were refined based on this tetragonal cell. This is illustrated by the XRD pattern of BNBT20 ($x = 0.20$) shown in Fig. 2b; here the inset shows the (0 0 2)/(2 0 0) peaks indicating the splitting of the cubic (2 0 0) reflection in the tetragonal phase.

The variation of the unit cell parameters in the system $(1-x)$ $Bi_{0.5}Na_{0.5}TiO_3$–x $BaTiO_3$ ($0 \leq x \leq 0.2$) for unpoled and poled samples (Table 1) is summarized in Fig. 3. For both sample sets, the rhombohedral cell expands with increasing x. At larger x, a transition into the tetragonal system is observed. For the unpoled samples, a morphotropic phase boundary is found in the range $0.06 \leq x \leq 0.08$. This is in good agreement with the MPB region reported by Takenaka.[4] For poled samples, a small, but significant change of unit cell dimensions is observed. In the rhombohedral range, the parameter a_{rh} is increased after poling, and the corresponding rhombohedral angles are somewhat reduced (Table 1). This is indicative of a stretching of the rhombohedral cell as a result of the poling treatment. A similar observation has been reported in Ref. [22] for the BNT–PT system; a shift of the peak positions between poled and unpoled rhombohedral samples was described. For the tetragonal compositions of the BNBT system we observe a significant increase of the parameter c_{tr} for the poled samples, whereas a_{tr} of poled samples is somewhat smaller compared to unpoled samples in the range $0.06 \leq x \leq 0.12$ and almost identical for purely tetragonal compositions. This also points to a stretching of the tetragonal cell in c-direction as a result of the poling treatment. Such shifts of peak positions after poling treatments have already been documented, e.g. for undoped PZT[18]; Klimov et al.[23] have reported changes in lattice parameters for Mn-doped PZT.

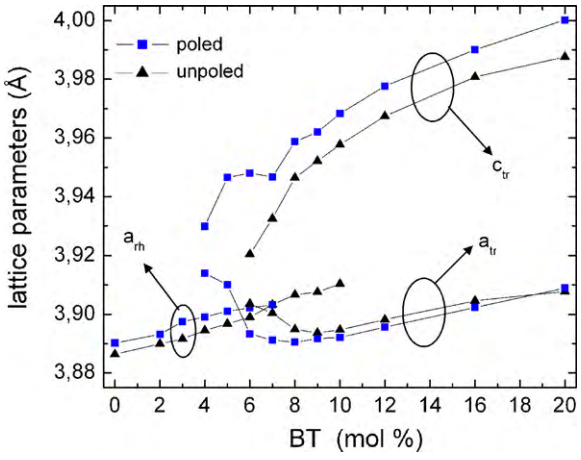

Fig. 3. Lattice parameters a_{rh}, a_{tr} and c_{tr} for $(1-x)$ $Bi_{0.5}Na_{0.5}TiO_3$–x $BaTiO_3$ with $0 \leq x \leq 0.2$ (0–20 mol% BT) for poled and unpoled samples.

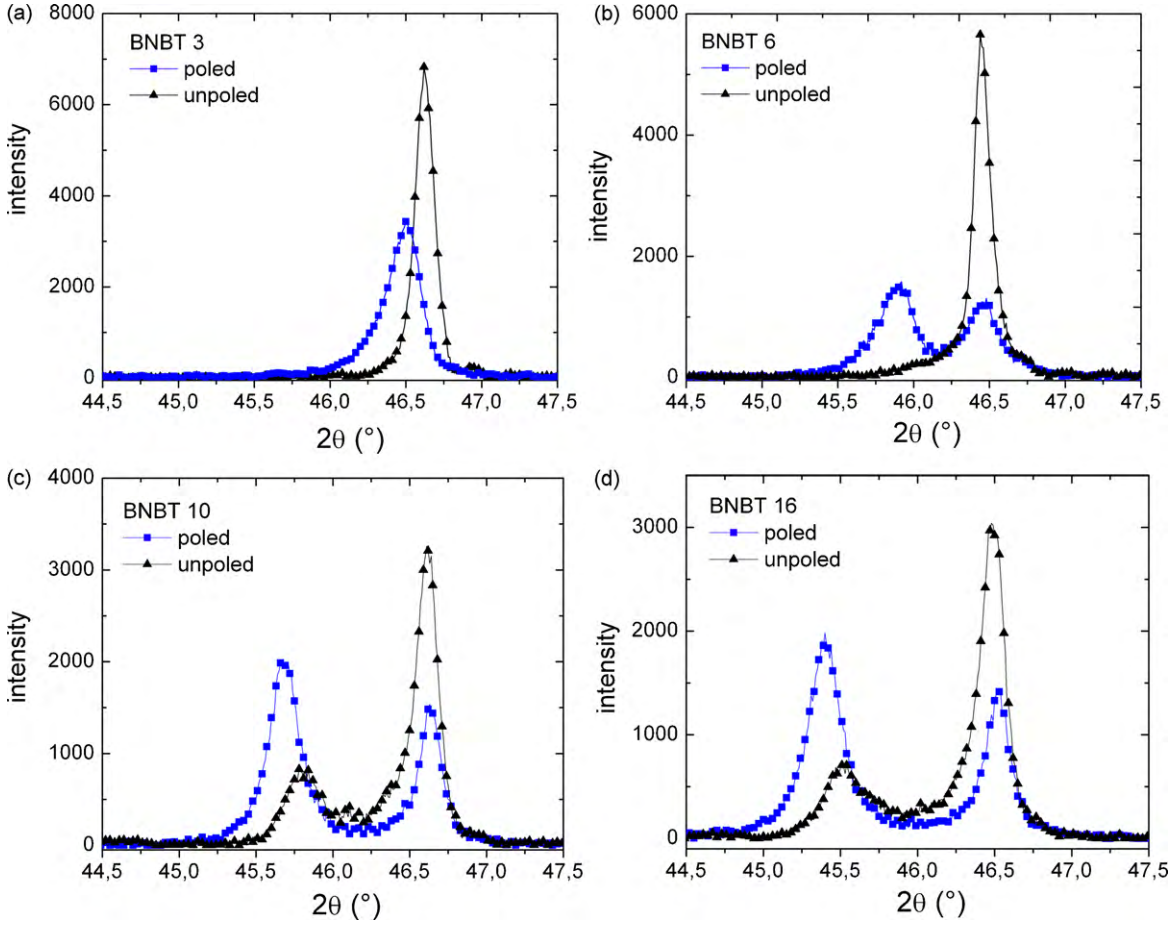

Fig. 4. XRD patterns of the pseudo-cubic (2 0 0) reflection for poled and unpoled samples of selected compositions: $x = 0.03$ (a), $x = 0.06$ (b), $x = 0.10$ (c), and $x = 0.16$ (d).

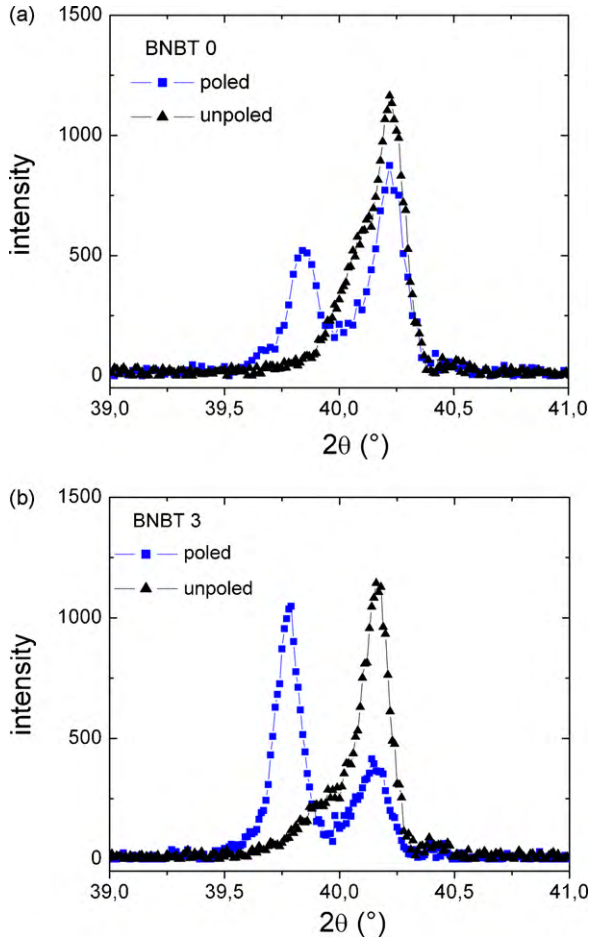

Fig. 5. XRD patterns of the pseudo-cubic (1 1 1) reflection for poled and unpoled samples of selected compositions: $x = 0$ (a), $x = 0.03$ (b).

A detailed description of the diffraction patterns of the pseudo-cubic (2 0 0) reflection of poled und unpoled ceramics is shown for four selected compositions in Fig. 4. For rhombohedral compositions, e.g. for BNBT 3, an immense change of the diffraction angle, the peak width and peak intensity is obvious after poling. For the tetragonal compositions, the typical splitting into (0 0 2) and (2 0 0) peaks is found. For unpoled ceramics, the intensity of the (0 0 2) reflection is smaller compared to the (2 0 0) reflection. In the poled state, an increase of intensity of the (0 0 2) peak compared to (2 0 0) is observed. This is expected, because poling causes a preferred orientation of the unit cells within the field direction. Moreover, in poled samples we observe a shift of the position of the (0 0 2) peak to larger lattice spacings. On the other hand, the peak position of the (2 0 0) reflection is almost constant. This behavior is consistent with the observed shift of lattice constants (Fig. 3). A remarkable change in the XRD patterns was found for the MPB composition BNBT6. As shown in Fig. 4, a clear tetragonal splitting of the (2 0 0) reflection occurs in the poled state.

A similar situation is found for the pseudo-cubic (1 1 1) peak: for the rhombohedral compositions $x = 0$ and 0.03 (samples BNBT0 and BNBT3) the reflections of poled samples show stronger splitting, different peak intensities and (1 1 1) peak positions (Fig. 5). This is again consistent with a stronger rhombohedral distortion (Fig. 3) and an orientation of the unit cells as a result of poling. The calculated lattice distortions (Fig. 6) reveal a rhombohedral distortion of about 0.5% in the unpoled and about 1% in the poled states, respectively. δ_{rh} tends to decrease as the BT-content x approaches the MPB region. The tetragonal distortion δ_{tr}, on the other hand, exhibits a strong enhancement with x; the increase is especially prominent across the morphotropic phase boundary. Poled samples also display a larger tetragonal distortion compared to unpoled samples; this increase of δ_{tr} is very large in the MPB region (e.g. from 0.5% to 1.5% for 6 mol% BT).

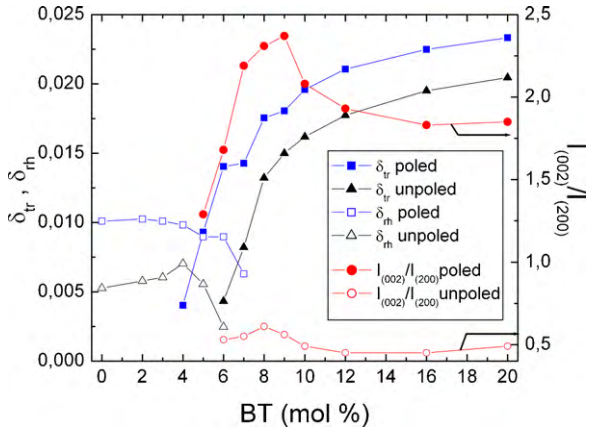

Fig. 6. Lattice distortions δ_{rh}, δ_{tr} and intensity ratio $I_{(0\,0\,2)}/I_{(2\,0\,0)}$ for poled and unpoled samples of the system $(1-x)$ $Bi_{0.5}Na_{0.5}TiO_3$–x $BaTiO_3$ with $0 \le x \le 0.2$ (0–20 mol% BT).

The intensity ratio of the tetragonal (0 0 2)/(2 0 0) peaks for poled and unpoled samples is also shown in Fig. 6. For the series of unpoled ceramics an almost constant intensity ratio of about 0.5 is found for all compositions with a significant amount of tetragonal phase ($0.06 \le x \le 0.20$). This might be interpreted as a signature of a random distribution of unit cell orientations, since twice the number of lattice planes in the tetragonal cell contributes to the (2 0 0) peak. For poled ceramics, however, a very pronounced increase of the intensity ratio signals a preferred orientation of the tetragonal cells along the direction of the poling field. Maximum intensity ratios are found to occur at the MPB.

The tetragonal volume fraction V_{tr} is shown for poled and unpoled samples as a function of composition x in Fig. 7. A dramatic increase of V_{tr} is found at the MPB region. For unpoled and poled samples, the tetragonal volume fraction of 50% appears at 7 mol% BT ($x = 0.07$) and 5 mol% BT ($x = 0.05$), respectively. Moreover, the variation of V_{tr} vs. BT-content x manifests significant differences between unpoled and poled samples. A dramatic change in the phase composition of the samples upon poling is demonstrated, which is again very pronounced in the MPB region. For example, at 6 mol% BT ($x = 0.06$) an impressive increase of V_{tr} from about 40–80% is observed. This implies that the majority of the material changes its structure from rhombohedral to tetragonal under the action of an electrical field. A large remanent strain of 0.25% was found from strain-field hysteresis curves.[13] Such behavior has not been observed in the BNBT system yet. It is also worth mentioning, that for unpoled ceram-

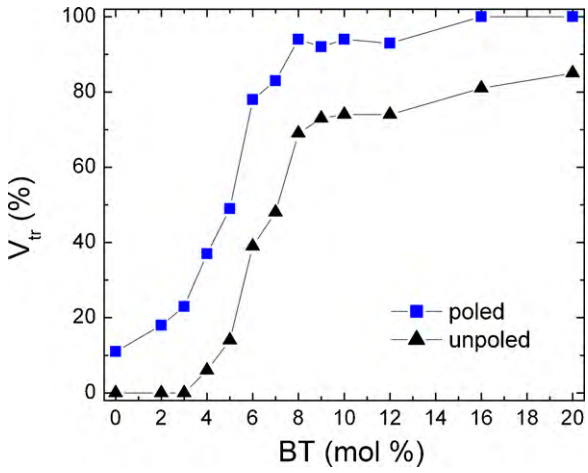

Fig. 7. Tetragonal phase content for poled and unpoled samples of the system $(1-x)$ $Bi_{0.5}Na_{0.5}TiO_3$–x $BaTiO_3$ with $0 \le x \le 0.2$ (0–20 mol% BT).

ics with large x, i.e. in the tetragonal compositional field, the used fitting routine results in quite solid concentrations of the rhombohedral volume fractions. This might be somewhat overestimated, however, inspection of the XRD patterns (e.g. for $x = 0.16$, Fig. 4d) clearly reveals a non-zero intensity between the tetragonal (0 0 2) and (2 0 0) peaks.

3.2. High-temperature XRD studies of poled and unpoled samples

The X-ray diffraction patterns of the tetragonal composition BNBT16 ($x = 0.16$) are shown for different temperatures in Fig. 8. In the unpoled state (Fig. 8a) the transition from a tetragonal structure at room temperature to a cubic cell is obvious for the diffractogram taken at $T = 250\,^{\circ}C$. For the poled samples (Fig. 8b) the same principal behavior is observed, however, a closer inspection reveals some important differences: (i) the tetragonal splitting is stronger in poled samples as expected from the variation of lattice parameters (Fig. 3), (ii) the tetragonal phase seems to persist up to higher temperatures as compared to the unpoled samples. At 300 °C, for example, the poled sample still displays the typical splitting of the (2 0 0) reflection, whereas the unpoled sample shows a diffraction pattern typical of a cubic perovskite. A more detailed study of the XRD patterns of BNBT16 as function of temperature (in steps of 10 °C) demonstrates, that for an unpoled sample (Fig. 9a) the tetragonal (0 0 2) and (2 0 0) peaks are clearly separated at 200 and 210 °C. Starting at 220 °C, the maximum peak intensity is found in the middle of the pseudo-cubic (2 0 0) group, combined with still detectable intensities at the tetragonal Bragg angles. At $T > 240\,^{\circ}C$ the only signal is the cubic (2 0 0) peak. The poled BNBT16 ceramics (Fig. 9b) clearly show a tetragonal structure up to 220 °C. The pattern recorded at 230 °C exhibits a weak signal at $2\theta = 46.3^{\circ}$ signaling the appearance of the cubic (2 0 0) reflection. However, additional tetragonal peak intensities are still observed up to about 300 °C, thus demonstrating a significant temperature range of a coexistence of tetragonal and cubic phases within the poled state. The results of the high-temperature XRD study of the tetragonal composition BNBT16 ($x = 0.16$) are

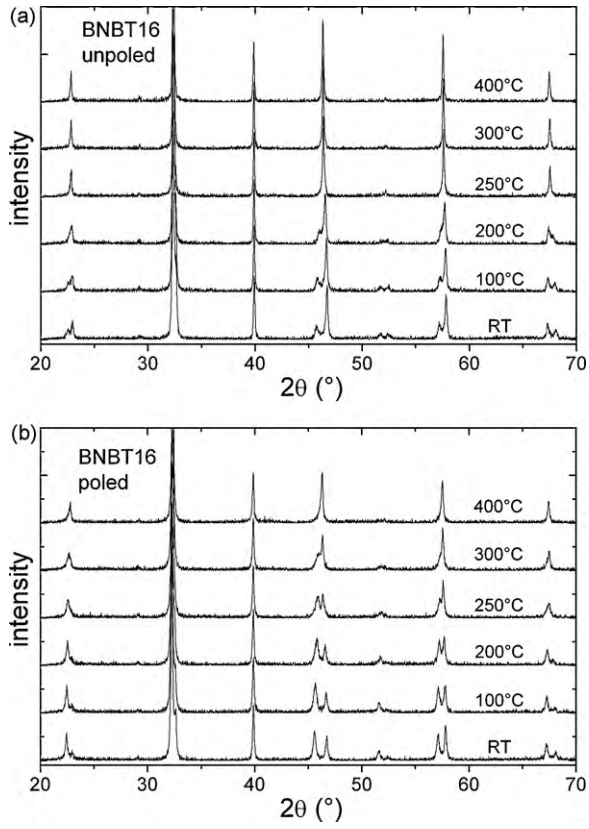

Fig. 8. XRD patterns of unpoled (a) and poled (b) samples of BNBT16 ($x = 0.16$) at various temperatures.

further supported by the variation of the tetragonal distortion for unpoled and poled samples (Fig. 10). The tetragonal distortion δ_{tr} decreases with increasing temperature, but for the unpoled ceramics δ_{tr} is reduced to small values at 230 °C. For the poled sample, at 230 °C a significantly larger distortion is found. At 300 °C a remarkable distortion of almost 0.01 is still present. Similarly, the tetragonal phase fraction (Fig. 10) in unpoled samples is reduced to practically zero at 250 °C, whereas for poled samples we still observe a remarkable concentration of almost 80% tetragonal phase at the same temperature. At 350 °C still about half of the poled samples volume consists of tetragonal phase. These findings demonstrate that tetragonal and cubic regions coexist over a wide temperature range.

Similar observation were made for sample BNBT7 ($x = 0.07$), a composition within the MPB region. For the unpoled sample (Fig. 9c), at 130 °C the main peak intensity is due to a somewhat rhombohedrally distorted phase. A very minor fraction of a tetragonal phase is present only; moreover, the tetragonal splitting is small. With increasing temperature a continuous transition to the cubic (2 0 0) peak proceeds. For the poled sample (Fig. 9d), on the other hand, as a result of a field induced transition a tetragonal phase with significant tetragonal distortion is the majority constituent at 130 °C. The appearance of a cubic peak is observed for the first time at 160 °C in addition to the tetragonal Bragg peaks. At higher temperatures, the volume fraction of the cubic phase increases. However, the cubic and tetragonal phases coexist up to about 350 °C (a low-angle tail of

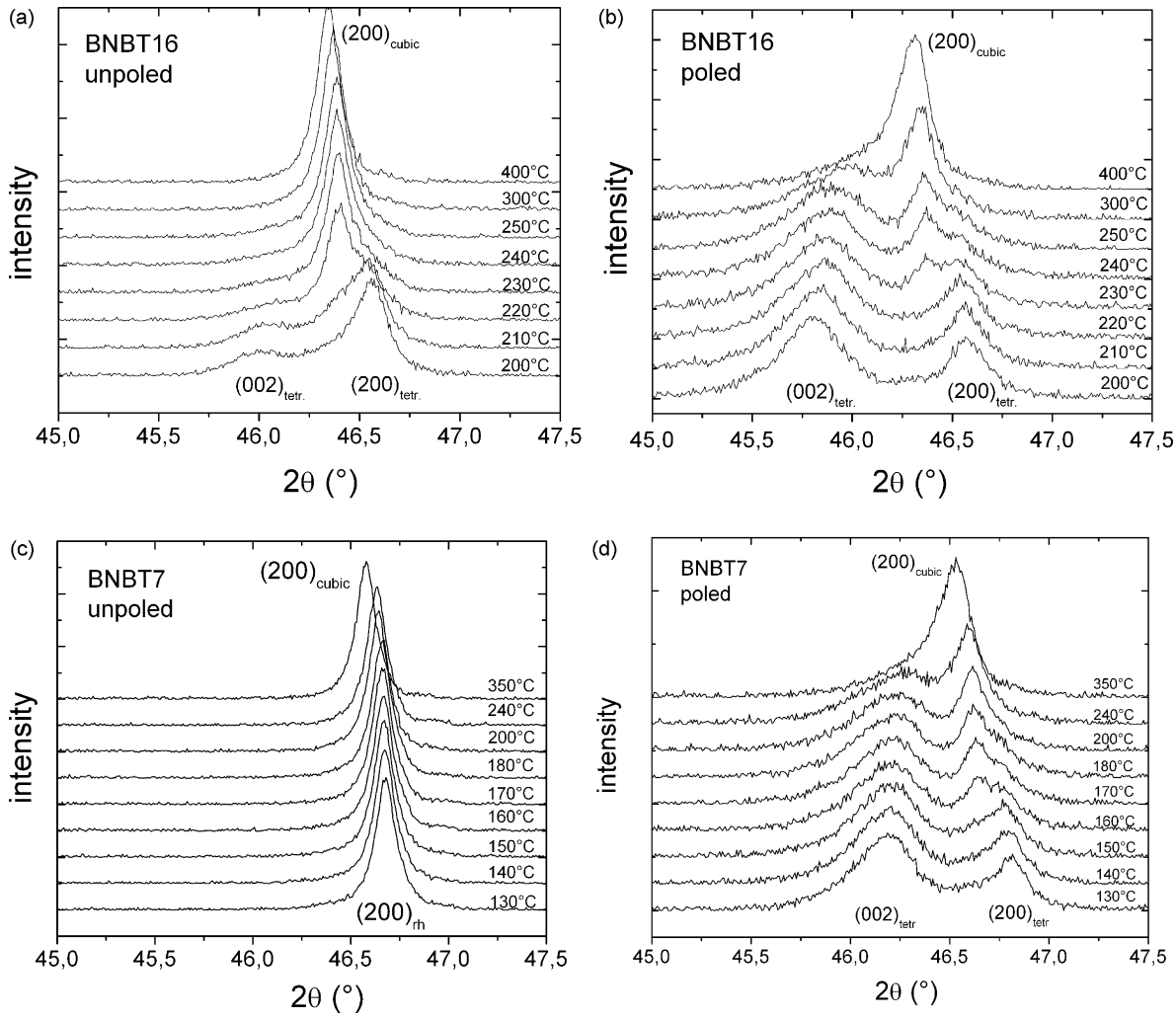

Fig. 9. XRD patterns of the pseudo-cubic (2 0 0) reflection for unpoled (a) and poled (b) samples of BNBT16 ($x = 0.16$) and unpoled (c) and poled (d) samples of BNBT7 ($x = 0.07$) at various temperatures.

the peak still indicates the presence of some tetragonal minority phase).

The results of the high-temperature XRD study of selected compositions are summarized in a tentative phase diagram of the system $(1-x)\,Bi_{0.5}Na_{0.5}TiO_3$–$x\,BaTiO_3$ ($0 \le x \le 0.2$) (BNBT). The changes in diffraction patterns of unpoled samples have not been further evaluated because of the strong peak overlap of compositions with weak tetragonal splitting. For predominantly tetragonal compositions (e.g. BNBT16), the tetragonal to cubic phase transition can be monitored. For poled samples, however, the temperature at which the cubic phase was detectable for the first time was taken as the tetragonal to cubic phase transition temperature T_{xrd}. These phase transformation temperatures are compared to data from electrical measurements[13] in Fig. 11. The data points were taken as T_m from the maximum in the capacitance vs. temperature curves and as T_d from the inflection points or kinks in the $C(T)$ curves of poled ceramics. The variation of T_m and T_d vs. composition x shown in Fig. 11 very well agrees with the original phase diagram as proposed in Refs. [4,24]. The transition temperatures T_{xrd}, determined in this study, are consistent with the data from electrical measurements. For compositions with 10–20 mol% BT ($0.1 \le x \le 0.2$), the transition to the cubic phase T_{xrd} coincides with T_m and T_d; see for example BNBT16 ($x = 0.16$). The $T_{xrd} = 220\,^{\circ}C$ reported for a composition with 12 mol% BT[17] fits well into the diagram. In the middle part of the

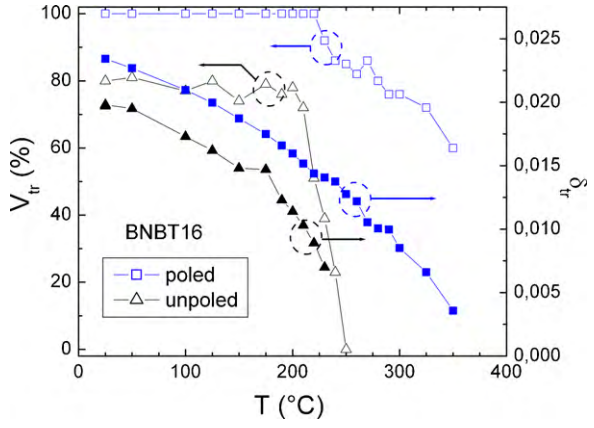

Fig. 10. Tetragonal volume fraction V_{tr} and tetragonal distortion δ_{tr} for unpoled and poled samples of BNBT16 ($x = 0.16$) as function of temperature.

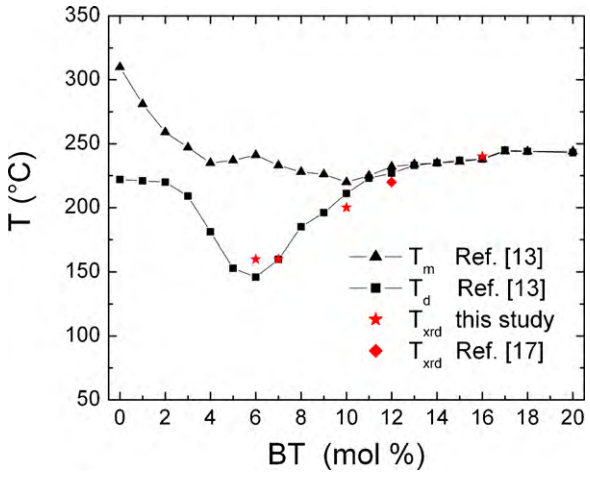

Fig. 11. Tentative phase diagram of the system $(1-x)$ $Bi_{0.5}Na_{0.5}TiO_3$–x $BaTiO_3$ with $0 \le x \le 0.2$ (0–20 mol% BT); T_m (temperature of capacitance maximum) and T_d (depolarization temperature; from inflection point or kink in the capacitance–temperature curve) are from Ref. [13]; T_{xrd} (temperature of cubic phase transition).

phase diagram, i.e. from 4 to 10 mol% BT ($0.04 \le x \le 0.1$) which includes the MPB region, T_m and T_d differ significantly. The depolarization temperature reaches a minimum value of 150 °C at $x = 0.06$. The measured T_{xrd} for $x = 0.06$, 0.07 and 0.10 support this compositional variation of transition temperatures. The evolution of electrical and electromechanical properties of a MPB composition with 6 mol% BT ($x = 0.06$) across the depolarization (T_d) and maximum (T_m) temperatures has been interpreted as transformations from the ferroelectric into an antiferroelectric and, at higher temperature, into a paraelectric phase.[12] The existence of an antiferroelectric state between T_d and T_m was proposed because of the appearance of a peculiar shape of the $P(E)$ curves with small remanent polarizations and a characteristic change in the bipolar $S(E)$ curves above T_d.[12] Whether an antiferroelectric order exists in that temperature range or not is still a matter of controversy; clear experimental proof of ordered sublattices is still lacking. The findings of our HT-XRD study in combination with our strain- and polarization-hysteresis measurements,[13] however, might be interpreted as a signature of a field induced phase transition or phase switching behavior. Similar conclusions were reported in a very recent paper by Daniels et al.[25] These authors have demonstrated by in situ synchrotron experiments that BNBT7 ($x = 0.07$) exhibits an electric field induced transition from pseudo-cubic to tetragonal.

4. Conclusions

We have performed a systematic XRD investigation of poled and unpoled lead-free $(1-x)$ $Bi_{0.5}Na_{0.5}TiO_3$–x $BaTiO_3$ ($0 \le x \le 0.2$) BNBT ceramics. A morphotropic phase boundary was confirmed at $0.06 \le x \le 0.08$. Differences in the unit cell parameters between poled and unpoled samples suggest a significant stretching of unit cells along the poling field direction. Dramatic changes of the peak intensities of the pseudo-cubic (2 0 0) and (1 1 1) reflections between poled and unpoled samples are interpreted by a significant increase of the tetragonal volume fraction in the poled state by a field induced phase transition. Temperature-dependent XRD studies of selected compositions confirm a transition to the cubic high-temperature phase. This phase transition temperature is in agreement with the depolarization temperature. However, at temperatures above the appearance of the cubic phase (cubic phase transition T_{xrd}) a significant fraction of the tetragonal phase coexists within the cubic phase field.

Acknowledgements

The authors thank Mr. M. Hofmann (HITK) for sample preparation and Dr. M. Müller (Univ. Jena) for help in HT-XRD measurements. Financial support of the project “LF-PICMA” from the state of Thuringia (Germany), co-funded by the European community within the EFRE program, is kindly acknowledged.

References

1. Moulson AJ, Herbert JM. *Electroceramics*. Chichester, UK: J. Wiley & Sons; 2003.
2. Shrout TR, Zhang S. Lead-free piezoelectric ceramics: alternatives for PZT? *J Electroceram* 2007;**19**:111–24.
3. Hennig E, Kolle B, Kynast A, Benkert K, Bathelt R, Soller T, et al. Status of lead-free piezoceramic materials. In: *Proceedings of the Actuator 2008, 11th International Conference on New Actuators*. 2008. p. 45–51.
4. Takenaka T, Maruyama K, Sakata K. $Bi_{0.5}Na_{0.5}TiO_3$–$BaTiO_3$ system for lead-free piezoelectric ceramics. *Jpn J Appl Phys* 1991;**30**:2236–9.
5. Chu BJ, Chen DR, Li GR, Yin QR. Electrical properties of $Bi_{0.5}Na_{0.5}TiO_3$–$BaTiO_3$ ceramics. *J Eur Ceram Soc* 2002;**22**:2115–21.
6. Gomah-Pettry JR, Said S, Marchet P, Mercurio JP. Sodium–bismuth titanate based lead-free ferroelectric materials. *J Eur Ceram Soc* 2004;**24**:1165–9.
7. Yoshii K, Hiruma Y, Nagata H, Takenaka T. Electrical properties and depolarization temperature of $Bi_{0.5}Na_{0.5}TiO_3$–$Bi_{0.5}K_{0.5}TiO_3$. *Jpn J Appl Phys* 2006;**45**:4493–6.
8. Takenaka T, Nagata H. Current status and prospects of lead-free piezoelectric ceramics. *J Eur Ceram Soc* 2005;**25**:2693–700.
9. Hiruma Y, Nagata H, Takenaka T. Phase transition temperatures and piezoelectric properties of $Bi_{0.5}Na_{0.5}TiO_3$–$Bi_{0.5}K_{0.5}TiO_3$–$BaTiO_3$ lead-free piezoelectric ceramics. *Jpn J Appl Phys* 2006;**45**:7409–12.
10. Watanabe Y, Hiruma Y, Nagata H, Takenaka T. Phase transition temperatures and electrical properties of divalent ions (Ca^{2+}, Sr^{2+} and Ba^{2+}) substituted $(Bi_{0.5}Na_{0.5})TiO_3$ ceramics. *Ceram Int* 2008;**34**:761–4.
11. Zhang ST, Kounga AB, Aulbach E, Granzow T, Jo W, Kleebe HJ, et al. Lead-free piezoceramics with giant strain in the system $Bi_{0.5}Na_{0.5}TiO_3$ $BaTiO_3$–$K_{0.5}Na_{0.5}NbO_3$. I. Structure and room temperature properties. *J Appl Phys* 2008;**103**:034107.
12. Zhang ST, Kounga AB, Aulbach E, Deng Y. Temperature-dependent electrical properties of 0.94 $Bi_{0.5}Na_{0.5}TiO_3$–0.06 $BaTiO_3$ ceramics. *J Am Ceram Soc* 2008;**91**:3950–4.
13. G. Picht. Diploma thesis. Germany: Univ. of Appl. Sciences Jena; 2006 [in German].
14. Jones GO, Thomas PA. Investigation of the structure and phase transition in the novel A-site substituted distorted perovskite compound $Na_{0.5}Bi_{0.5}TiO_3$. *Acta Cryst* 2002;**B58**:168–78.
15. Isupov VA. Ferroelectric $Bi_{0.5}Na_{0.5}TiO_3$ and $Bi_{0.5}K_{0.5}TiO_3$ perovskite and their solid solutions. *Ferroelectrics* 2005;**315**:123–47.
16. Suchanicz J, Kwapulinski J. X-ray diffraction study of the phase transition in $Bi_{0.5}Na_{0.5}TiO_3$. *Ferroelectrics* 1995;**165**:249–53.
17. Suchanicz J, Kusz J, Böhm H, Stopa G. Structural and electric properties of $(Bi_{0.5}Na_{0.5})_{0.88}Ba_{0.12}TiO_3$. *J Mater Sci* 2007;**42**:7827–31.
18. Guo R, Cross LE, Park SE, Noheda B, Cox DE, Shirane G. Origin of the high piezoelectric response in $PbZr_{1-x}Ti_xO_3$. *Phys Rev Lett* 2000;**84**:5423–6.

19. Kungl H, Theissmann R, Knapp M, Baehtz C, Fuess H, Wagner S, et al. Estimation of strain from piezoelectric effect and domain switching in morphotropic PZT by combined analysis of macroscopic strain measurements and synchrotron X-ray data. *Acta Mater* 2007;**55**:1849–61.
20. Geller S, Bala VB. Crystallographic studies of perovskite-like compounds. II. Rare earth aluminates. *Acta Cryst* 1956;**9**:1019–25.
21. Moreau JM, Michel C, Gerson R, James WJ. Atomic displacement relationship to rhombohedral deformation in some perovskite-type compounds. *Acta Cryst* 1970;**B26**:1425–8.
22. Kuharuangrong S, Schulze W. Characterisation of $Bi_{0.5}Na_{0.5}TiO_3$–$PbTiO_3$ dielectric materials. *J Am Ceram Soc* 1996;**79**:1273–80.
23. Klimov VV, Ponomarjev Y, Didkovskaja OS, Salev VS. Investigation of piezoceramics for piezotransformers. *Ferroelectrics* 1978;**17**: 501–3.
24. Himura Y, Yoshii K, Nagata H, Takenaka T. Investigation of phase transition temperatures on $Bi_{0.5}Na_{0.5}TiO_3$–$Bi_{0.5}K_{0.5}TiO_3$ and $Bi_{0.5}Na_{0.5}TiO_3$–$BaTiO_3$ lead-free piezoelectric ceramics by electrical measurements. *Ferroelectrics* 2007;**346**:114–9.
25. Daniels JE, Jo W, Rödel J, Jones J. Electric field induced phase transformation at a lead-free morphotropic phase boundary: case study in a 93% $Bi_{0.5}Na_{0.5}TiO_3$–7% $BaTiO_3$ piezoelectric ceramic. *Appl Phys Lett* 2009;**95**:032904.